Delft University of Technology
Master of Science Thesis in Embedded Systems

Underwater 3D localization and communication for mobile networked robots

Daniel van Paassen

TU Delft Delft University of Technology

Underwater 3D localization and communication for mobile networked robots

Master of Science Thesis in Embedded Systems

Networked Systems group
Faculty of Electrical Engineering, Mathematics and Computer Science
Delft University of Technology
Van Mourik Broekmanweg 6, 2628 XE Delft, The Netherlands

Daniel van Paassen

24th January

Author
Daniel van Paassen

Title
Underwater 3D localization and communication for mobile networked robots

MSc Presentation Date
29th January 2024

Graduation Committee

dr. R. R. Venkatesha Prasad (direct supervisor)	Delft University of Technology
prof. dr. ir. G.N. (Georgi) Gaydadjiev	Delft University of Technology

The work in this report has been made into a paper which is to be submitted for application at the ACM SIGCOMM 2024.

Abstract

Localization for autonomous underwater vehicles (AUVs) is still an ongoing challenge because of the lack of usability of methods such as GPS. We researched a localization method for an AUV swarm with the possibility of communication using the same channel. This uses an Angle of Arrival (AOA) together with the Received Signal Strength Ratio (RSSR) on blue LED signals. The localisation's workings are invariant to the absorption coefficient of different waters due to the absence of absolute Received Signal Strength (RSS). It enables swarm behaviour for these robots at a low cost by providing them with relative localization and the possibility of having the blue LED signal link as a high-bandwidth communication channel. This system has a confidence label that relates well to the accuracy of the measurements, with the best one giving a Mean Absolute Error (MAE) of 3.1 cm at 32 cm distance and 39 cm MAE at 1 meter, all taken at 100Hz. Additionally, it has the possibility to communicate in the kbps range.

Preface

This thesis marks my last stone from finishing my Master's at TU Delft University. It has been a rewarding experience where I could apply my learned skills and put myself towards a long goal of contributing to technological advances

I am grateful for the support from my supervisors, Suryansh Sharma, and Dr. Rango Rao Venkatesha Prasad for guiding me through this project. I additionally want to thank everyone else who supported me and who were willing to hear my monologue-style sparring sessions.

Daniel van Paassen

Delft, The Netherlands
24th January 2024

Contents

Chapter 1

Introduction

Autonomous underwater vehicles (AUVs) have broad applicability in aquatic environments and other applications. These range from the mapping of the 3D underwater environment [34], detection of mines [2] to the inspection and monitoring of ports [39]. Such applications benefit from having cost-effective and autonomous swarms of underwater vehicles that can carry out such sensing tasks and communicate the information back to the surface. To this end, good communication and localization between these underwater systems is needed. Homogeneous groups of underwater mobile robots need to both relatively localize other robots and establish communication links within the group. This can enable implicit coordination, swarming behaviours and more efficient control [13]. Collaborative AUV missions can indeed propel such applications. However, they require a method for fast intra-swarm localization [25].

1.1 Underwater localization and communication

The underwater environment is challenging when viewed from the traditional communication channel lens. This is due to water's higher absorption and scatter properties compared to air [38]. This renders radio frequency-based communication and localization systems practically unusable inside the water [44]. We are, thus, forced to look at alternative non-radio-based modalities that can work in aquatic environments.

Acoustics are a viable alternative, especially for long distances (in kilometres range) because of their low absorption rate underwater. However, they perform poorly in shallow waters due to acoustic reflections from the surface and bottom [27]. Orthogonal Frequency Division Multiplexing (OFDM) based acoustic communication links can also contain large impulsive noise [11]. Additionally, acoustic links have been reported to affect marine life and can be pretty intrusive to such ecosystems [10]. This is a critical consideration, especially for marine life monitoring. Acoustics can be a good solution for enabling long-range communication links but are relatively

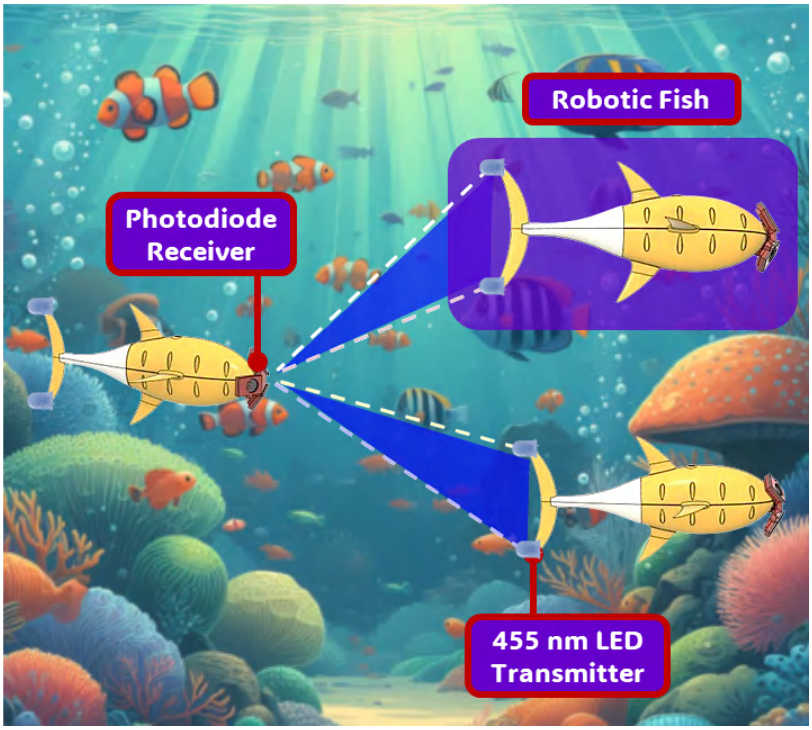

Figure 1.1: **Multiple robotic fishes using the localization system with transmitters on the tail and a receiver structure in the front.**

expensive when used in short-range [36].

On the other hand, optical light signals in the fluorescent light spectrum have a larger bandwidth for ranges up to 10 m as compared to radio or acoustic signals [42]. This, however, differs in different waters, with 450 nm being the least attenuated in the open ocean, which shifts to 540 nm for dirtier waters [42]. These systems have been demonstrated to work in the context of underwater communication. Still, they experience signal multi-path, especially near the sea bed or surface [35] and are subject to the water's turbidity [4]. Light-based underwater systems can be a potential option for underwater robots if they conform to the limitations such robots impose on the system.

1.2 Challenges and Requirements

Underwater mobile robots need to operate in challenging environmental conditions that impose certain system limitations on their communication and localization methodology. Such robots, especially untethered ones, have a strict power budget due to limited onboard battery. Conserving battery life is, thus, of great importance. An-

other consideration is that such systems are often compact in size and have resource constraints regarding space and computing. Since mobile underwater robots are typically 50-150 cm big, we need a system that can localize and communicate well within a couple of meters. This should be possible in different water turbidity and visibility conditions. The effects of the channel on marine life should also be considered, as acoustic signals have the disadvantage of potentially harming marine life. In contrast, optical and RF do not have known adverse effects on marine life [51].

Key requirements we elicit are therefore: ① the system should be low power to consume as little energy as possible; ② be compact and space efficient while enabling onboard robot-robot coordination, joint communication, and sensing should be performed. This limits the number of different subsystems required in the robots. ③ it must localize and communicate with other robots in 3D for a range of at least a few meters to reach drones operating in the shared physical space. ④ we should only rely on the constrained resources found in underwater robots of this scale, thus limiting processing overhead, energy consumption, and additional weight. ⑤ the operational environment should be independent of water quality and turbidity. This allows for a more widespread applicability.

1.3 Our System

We introduce a system where simultaneous localization and communication are possible by using two blue 455 nm LEDs as transmitters in combination with a specially designed photodiode (PD) array structure as receiver on each AUV. This is depicted in Fig. 5.1. An advantage of using optical light communication would be the reduced power consumption on smaller distances due to the availability of efficient and compact optical devices [32].

1.3.1 LED based implicit localization, explicit communication

We place two blue LEDs vertically on the underwater robot. By knowing the separation of the LEDs and their angles relative to a distant observer, we can estimate a robot's 3D location[13]. The angles are inferred using the Received Signal Strength Ratio (RSSR), eliminating the need for extensive calibration. This is required in other methods like distance estimation using RSS, which uses signal strength to characterize link attenuation. In our case, different waters with different scatter and absorption rates can be used with the same system. The two vertical LEDs are placed on the tail of each AUV and act as transmitters for both localization and communication.

1.3.2 Photodiode-based inferencing

Instead of cameras to deduce the location of the LEDs like other works in literature, we use a three-photodiode array structure with an angular separation between the diodes [49]. This method might be less accurate than a camera, but it can infer the location an order of magnitude faster while requiring less energy to do so [14]. This high-speed inferencing allows us to encode data effectively using the LEDs as optical transmitters and establish a communication channel on top of localization. For the PDs, the OPT101 module is used [30]. We use different frequencies for each LED to enable the receiver system to distinguish them. Additionally, our system allows for Frequency Shift Keying (FSK) or other optical OFDM-based modulation schemes to be used in conjunction. This facilitates explicit communication over the same channel. Our system requires a Line Of Sight (LOS) between the observer and the robot. This LOS is not expected to break often for an underwater robotic swarm. A Kalman filter can also be used to update the swarm robots' positions accurately.

We summarize the key contributions as follows:
(1) Theoretical Modelling of the optical channel between an LED and PD, including the effect of the receiver's physics and the channel's length, i.e., the distance between the transmitter and receiver. The angles of a blue LED pair on a tail can then be used to find the 3D relative position of that tail, illustrated in Chapter 3;
(2) A novel localization system design that aims to provide a low power, low complexity localization method for underwater robots with a provision for joint communication and localization using a training free learning algorithm, discussed in Chapter 5;
(3) Experimental dataset building upon the first two contributions, provides extensive characterization of the localization system, described in Chapter 6, along with a discussion of adapting it for different types of underwater conditions in Chapter 7.

Our system can localize objects at 100 Hz rate with an MAE of 3.2 cm at 32 cm at high confidence levels and is designed to operate up to a distance of 1 meter robot-robot separation. It takes 237 mW to operate. The system is implemented for the open-source bio-inspired fish robot OpenFish [12], augmenting it with localization and communication possibilities to enable swarming behaviour. However, it finds applicability in a wide range of AUVs.

Chapter 2

Related work

Our work touches upon several interrelated areas. We briefly survey relevant works below. Although there is significant prior work on underwater communication and messaging using both acoustic [20, 43] and optical modalities [3, 52], we focus primarily on underwater localization.

2.1 Underwater 3D localization

There exists great interest in tracking both static sensors and mobile robots underwater [29, 48, 21]. One well-researched area is to use acoustic pressure waves from floating buoys that act as anchors to estimate location using time of arrival [16], time difference of arrival [19], angle of arrival [28] or received signal strength [37]. These leverage acoustic pulse waves to perform ultra short baseline [41] and long baseline positioning [47]. Such methods can estimate both distances and angles but leverage existing infrastructure, are often power hungry and large sized, which limits their deploy-ability, especially for resource-constrained mobile robots [47].

2.2 Tracking underwater mobile targets

Different anchor-based methods that aim to create an underwater GPS have been explored for tracking smaller mobile targets inside water. Some methods use hydrophone beaconing devices on the water surface to communicate and locate underwater divers [31, 9]. In contrast, another uses the divers' smart watches for relative localization by combining acoustic signals with pairwise equation solving [18]. Another work that proposes the use of an underwater pinging device requires a high-precision GPS synchronized clock [5]. Surface buoys themselves have also been augmented with GPS to provide tracking inside water [6].

Other methods focusing on underwater autonomous vehicles estimate position based on time of arrival measurements [16] or using specialized directional beacons [33]. These are not well suited for low-power, small-sized robots and often require a separate communication system. Another approach involves using underwater backscatter to enable battery-free nodes. However, they only give 1-dimensional positioning [24].

2.3 Visible light localization

Researchers have found that sound-based acoustic positioning systems can have a detrimental and hazardous impact on marine and amphibious life [40, 23]. Further, acoustic localization can be very effective for long distances. Still, for smaller distances, they are inadequate, especially in the purview of the safety of the mobile systems, which requires higher accuracy and update rates [15]. These reasons, combined with the high bandwidth communication that underwater visible light-based systems offer [7], make such systems an attractive alternative to acoustic-based ones for swarm topologies.

We know from the vast body of literature that complex 3D swarming behaviour in nature stems from making visual observations of nearby neighbours without any explicit communication [13]. A well-established underwater visible light localization approach is, thus, to use cameras with LEDs acting as active markers. Such systems can track multiple simultaneous robots with high accuracy and speed at short distances [15]. These computer vision systems are relatively power-hungry and provide extremely slow tracking refresh rates in the order of a few Hz.

Unlike cameras, photodiode (PD) based systems can enable rapid robot localization and simultaneous communication. This has been well tried on land with different PD structures [26]. Different indoor methods have used different physical parameters to extract localization information from LED light signals and multi-directional PDs [45, 46, 50]. In particular, PD-based indoor visible light communication systems use RSS for 3D localization [49] and have not been explored for underwater localization. Our system provides a method of implementing 3D localization utilising an array of multi-directional photodiodes that can localize underwater robots even in varying water visibility conditions.

Chapter 3

Modelling Visible Light Links

We explain here the theoretical background of our work and build the foundation that guides us in our design choices for the localization system. We model the optical channel between an LED and PD using the physics behind light propagation. This enables us to create a database of RSSR values between the different PDs for a given LED distance and orientation. This can be used to contrast and compare the experimentally measured received power. Such a database can thus be used to deduce the relative direction of the transmitting LED.

3.1 Channel Configuration

The system considers a blue LED pair mounted on a robotic fish's tail (which can be generalized to the rear) as the transmitter. All coordinates are referenced to the centre point of the photodiode receiver structure, with each PD having its own optical filter. The possible blue LED locations and the three photodiode vectors are depicted in Fig. 3.1 for a 300 mm horizontal distance. For a known distance, by calculating the orientation angle of the pair of LEDs, we can find the relative 3D position of the transmitter.

The model is derived using the physics of the PDs, their position and the channel length, i.e., the distance between the transmitter and receiver. The following equation shows the received power of a blue LED with LOS at each PD:

$$P_{\mathrm{r},i,j} = C \cdot G_{\mathrm{r}}(\theta_{i,j}) \cdot G_{\mathrm{t}}(\lambda_{i,j}) \cdot \frac{P_{\mathrm{t},j}}{4\pi(d_{\mathrm{i,j}})^2}. \tag{3.1}$$

Here, each PD is denoted with i ($\forall i \in \{A, B, C\}$), and each LED with j ($\forall j \in \{1, 2, ..., N\}$) for an even number of N. Every fishtail will have two LEDs, as explained in Section 5.2. For this, we denote f ($\forall f \in \{1, 2, ..., N/2\}$), where each f would have a f_t and f_b to indicate the top and bottom LED respectively.

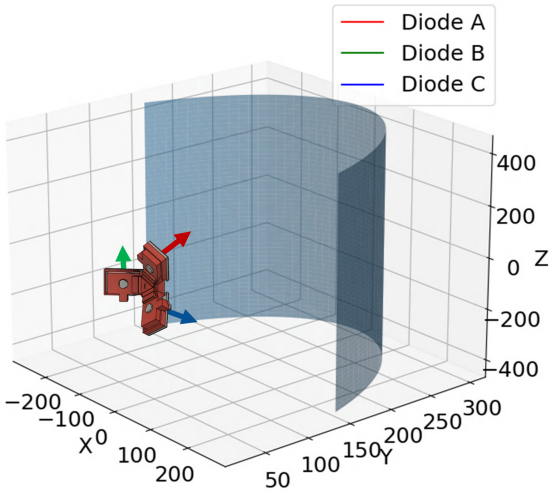

Figure 3.1: **Coordinate system modelled with LEDs at a horizontal distance of 300 mm.**

$P_{\mathrm{r},i,j}$ stands for the received light power at the PD with index i coming from the LED with index j. C is a constant factor of attenuation of the glass filter, assumed to be the same for all PDs. G_{r} is the gain at the diode dependent on angle θ. $\theta_{i,j}$ is the angle of the light ray coming from LED j to PD i, compared to the normal vector of the PD i. G_{t} is the gain factor of the LED transmitter. This term depends on $\lambda_{i,j}$, the angle that the light ray from j to i has compared to the normal vector of the LED j. $P_{\mathrm{t},j}$ is the transmitted power by LED j. The last variable is the distance between PD i and LED j. It is important to note that these gains also depend on the wavelength of the transmitted light. However, we only consider blue 455 nm wavelength light and, thus, have not included that factor in these equations.

3.2 PD Receiver Physics

For the PDs, the angle over which the light is coming from, with respect to the length or width of the die, has a different response due to diffraction and scattering in the package (see Fig. 3.2). In practice, this difference was negligible when measuring over both angles. The response was measured in air and fitted to the model with a third-order polynomial. This is the only calibration step required for our method.

To calculate angle $\theta_{i,j}$, the vector $\mathbf{r}_{i,j}$ between the LED j and PD i is calculated with:

$$\mathbf{r}_{i,j} = \mathbf{v}_j - \mathbf{v}_i. \tag{3.2}$$

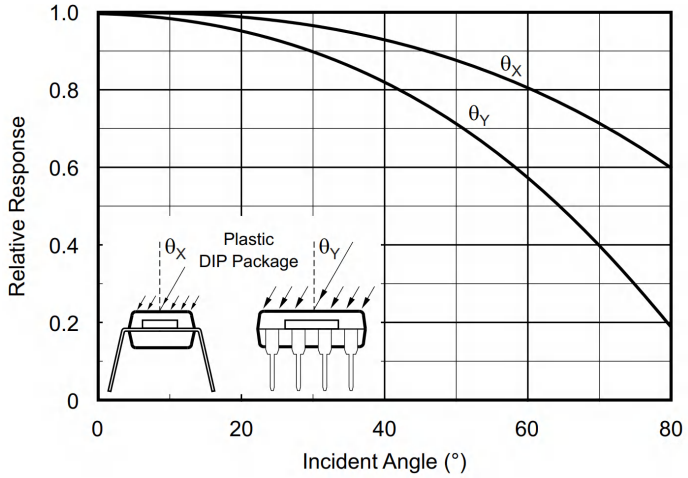

Figure 3.2: **Relative response curve with varying incident light angle of the OPT101 [30]**

Where:

$$\mathbf{r}_{i,j} = \begin{bmatrix} \mathbf{r}_{i,j,x} \\ \mathbf{r}_{i,j,y} \\ \mathbf{r}_{i,j,z} \end{bmatrix} \text{ is the vector from the LED } j \text{ towards PD } i,$$

$$\mathbf{v}_j = \begin{bmatrix} \mathbf{v}_{j,x} \\ \mathbf{v}_{j,y} \\ \mathbf{v}_{j,z} \end{bmatrix} \text{ is the vector from origin towards LED } j,$$

$$\mathbf{v}_i = \begin{bmatrix} \mathbf{v}_{i,x} \\ \mathbf{v}_{i,y} \\ \mathbf{v}_{i,z} \end{bmatrix} \text{ is the vector from origin towards PD } i.$$

The resulting vector is then used to calculate the angle between the light ray falling in PD i and the direction the PD faces:

$$\theta_{i,j} = \arccos\left(\frac{\mathbf{d}_i \cdot \mathbf{r}_{i,j}}{\|\mathbf{r}_{i,j}\|}\right). \tag{3.3}$$

Here, $\mathbf{d}_i$ is the unit vector in the direction that the PD is facing. Finally, for the d_{ij} element of Eq. (3.1), $\|\mathbf{r}_{i,j}\|$ is used.

3.2.1 Angle Estimation Using Multiple PDs

We take the ratio of the received powers between two PDs for the same LED. This is converted then converted to a logarithmic scale. We term this RSSR as $\Delta_{AB,j}$ for the

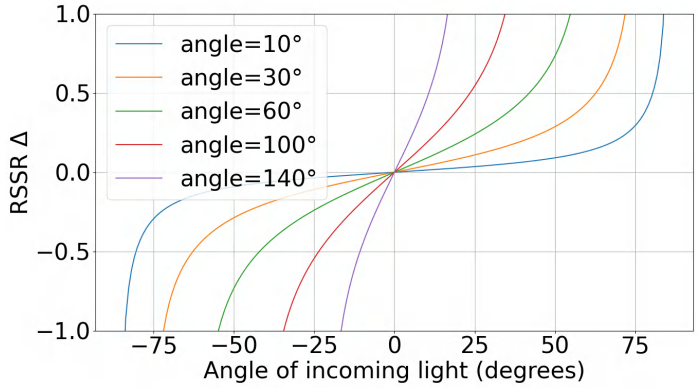

Figure 3.3: **Δ for a pair of photodiodes with varying angle difference between them in 2D space (Eq. (3.5)).**

ratio between two PDs PD_A and PD_B for LED j. This can be seen in the following equation for all PD combinations:

$$\begin{aligned}\Delta_{i,k,j} &= \log(P_{\mathrm{r},i,j}) - \log(P_{\mathrm{r},k,j}) \\ &= \log\left(\frac{G_{\mathrm{r}}(\theta_{i,j})}{G_{\mathrm{r}}(\theta_{k,j})}\right) + \log\left(\frac{G_{\mathrm{t}}(\lambda_{i,j})}{G_{\mathrm{t}}(\lambda_{k,j})}\right) \\ &+ \log\left(\frac{d_{i,j}^2}{d_{k,j}^2}\right) \forall (i,k) \in \{(A,B),(A,C),(B,C)\}.\end{aligned} \tag{3.4}$$

Due to the small distance between each PD, $\lambda_{i,j}$ can be approximated to be equal to $\lambda_{k,j}$. Also, $d_{k,j}$ can be approximated to be equal to $d_{i,j}$ since the difference in distance between the PDs is negligible compared to the total distance to the LED. This reduces the equation to:

$$\Delta_{i,k,j} = \log(P_{\mathrm{r},i,j}) - \log(P_{\mathrm{r},k,j}) = \log\left(\frac{G_{\mathrm{r}}(\theta_{i,j})}{G_{\mathrm{r}}(\theta_{k,j})}\right). \tag{3.5}$$

The way the PDs are oriented in the receiver structure is critical. By changing the angle difference between the PDs with respect to each other, we can change the response derived from Eq. (3.5). This is demonstrated in Fig. 3.3 for a 2D space, assuming the PDs are in the same physical space, and only the tilt is different. By adjusting this relative orientation of the PDs, we can affect the total Field Of View (FOV) that the receiver captures. The FOV seen in the Fig. 3.3 can be approximated with:

$$\mathrm{FOV} = 180^\circ - \arccos\left(\mathbf{d}_i \cdot \mathbf{d}_k\right). \tag{3.6}$$

where the arccos term is the angle difference of the direction vectors between a PD pair. For the three PDs, the usable part between the three PD pairs will be only the

overlapping part between the FOV of each pair, resulting in a smaller FOV. Moreover, the FOV will be smaller when the PDs are separated from each other, in cases where the light source is relatively close by.

This highlights an important trade-off between having a larger FOV or a higher gradient in the received power of the transmitter LED. A steeper change in incoming light power would give a greater Δ (RSSR) value, making it more robust to noise. Especially for small angle differences in Fig. 3.3, the gradient of the log of the division does not vary significantly at the centre of the graph.

Δ is currently defined as a power ratio in bel (B), so for visualization purposes we convert this to dB with $10 \cdot \Delta$. The result of the RSSR in dB for the three PDs with a 35-degree tilt with respect to the receiver's normal vector (as seen in Fig. 3.1) can be found in Fig. 3.5. The values -4, -2 and -6 dB are highlighted in the graphs (a), (b), and (c) respectively. This indicates what the input could be at the PDs. Do note that in practice, these values can have a shift in the dB values, and not all scenarios will have 0 dB as the strongest signal. This is subject to the separation distance of the LEDs from the receiver, amongst other factors. Also, note that all values only until -12 dB are shown for readability. Lower received powers than -12 are not excluded by the system in the application.

The yaw and pitch offset shown on the axes of the graphs represent the transmitter angles as indicated in Fig. 3.4. These are calculated with:

$$\theta_{\mathrm{y},j} = \sin^{-1}\left(\frac{\mathbf{v}_{j,x}}{\|\mathbf{v}_{j,x,y}\|}\right). \tag{3.7}$$

The pitch is calculated with:

$$\theta_{\mathrm{p},j} = \tan^{-1}\left(\frac{\mathbf{v}_{j,z}}{\|\mathbf{v}_{j,x,y}\|}\right). \tag{3.8}$$

In these two equations, $\theta_{\mathrm{y},j}$ stands for the yaw offset and $\theta_{\mathrm{p},j}$ for the pitch offset.

While the graphs in Fig. 3.5 show the variation of the received power in individual PDs, the result of their combination is shown in the plots of Fig. 3.6b. This is done by subtracting the different PD Δ found using Eq. (3.5). The resultant values from each PD pair are then mapped on top of each other in the same plot. The red lines indicate a specific highlighted value of Δ for each PD pair that is meant to represent a specific measured value found experimentally.

We can see from Fig. 3.6b that only one unique yaw and pitch offset combination exists when comparing the measured values from the three PD pairs (AB, AC and BC). This is represented by the intersecting point of the three red lines. Note that although only using two diode pairs is already sufficient to arrive at a unique yaw, pitch coordinate; including a third one adds more robustness to where the intersection should be.

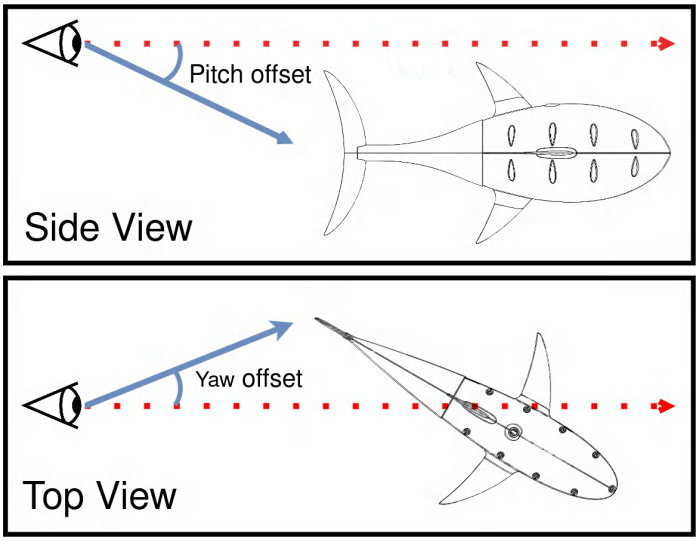

Figure 3.4: **Side and top view showing pitch and yaw offsets of an underwater robot with respect to a distant observer.**

3.3 Distance & 3D Position Estimation

Once the 2D orientation of both the top and bottom LEDs has been found (f_t and f_b), the horizontal distance to the LEDs can be estimated. This would correspond to the Y-axis length between the receiver and the transmitter in Fig. 3.4. Using the knowledge of the LED placement, we can calculate this distance using:

$$\begin{aligned} \|\mathbf{v}_{f.\mathrm{t},z} - \mathbf{v}_{f.\mathrm{b},z}\| = (\tan(\theta_{\mathrm{p},f.\mathrm{t}}) + \tan(-\theta_{\mathrm{p},f.\mathrm{b}})) \\ \cdot \|\mathbf{v}_{j,x,y}\|. \end{aligned} \tag{3.9}$$

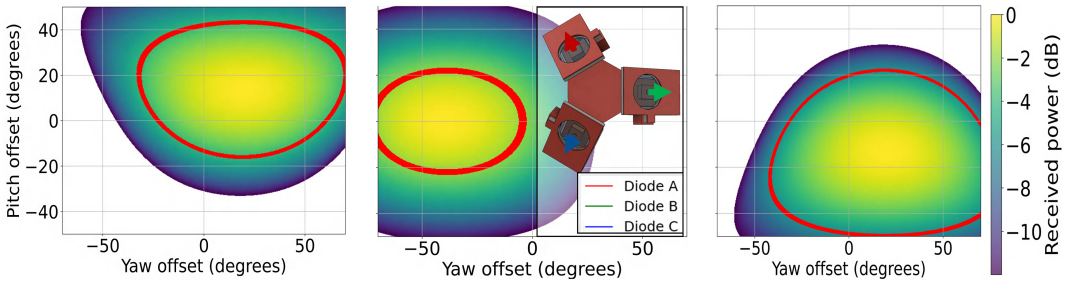

(a) **Photodiode A with highlighted value -4.** (b) **Photodiode B with highlighted value -2.** (c) **Photodiode C with highlighted value -6.**

Figure 3.5: **Received power for all PDs for all yaw and pitch offsets at a distance of 30 cm. The vertical ticks and colour bar values are shared.**

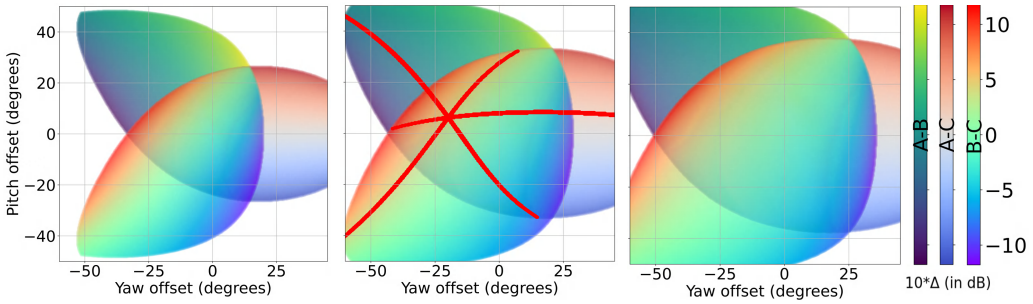

(a) **At 15 cm.** (b) **At 30 cm.** (c) **At 150 cm.**

Figure 3.6: **RSSR Δ plots for each diode pair AB, AC and BC with different horizontal LED-receiver distances. The vertical ticks and colour bar values are shared.**

Here, $\|\mathbf{v}_{j,x,y}\|$ represents the horizontal distance between the receiver and LED, and $\|\mathbf{v}_{f.\mathrm{t},z} - \mathbf{v}_{f.\mathrm{b},z}\|$ is the vertical distance between the two LEDs on a robot (tail). We can rewrite this equation to find the horizontal distance of the tail:

$$\|\mathbf{v}_{j,x,y}\| = \frac{\|\mathbf{v}_{f.\mathrm{t},z} - \mathbf{v}_{f.\mathrm{b},z}\|}{\tan(\theta_{\mathrm{p},f.\mathrm{t}}) + \tan(-\theta_{\mathrm{p},f.\mathrm{b}})}. \tag{3.10}$$

From Fig. 3.6, we see that the Δ plots depend highly on the distance between the LEDs and the receiver. This is due to the resultant vector as seen in Eq. (3.2). If the PDs were located in the same physical 3D space, it would result in $\mathbf{r}_{i,j} = \mathbf{v}_j$, and the ratio plot would only depend on the direction vector of the PDs. Since this is not the case, the following problem arises: We need to know the horizontal separation between the LEDs and receiver to generate the Δ plots. However, the horizontal distance calculation needs the Δ plots to find the angles relative to the top and bottom LEDs. This is solved using an algorithm described in Algorithm 1. Here, a subtraction pair A-B would mean that the logarithmic output from diode B is subtracted from diode A; distance stands for the horizontal distance between the receiver and the transmitter. In brief, the algorithm first uses an initial distance to generate the plot, we label this `db_distance`; then, the resulting LED angles are used to estimate the distance, and a new distance estimate is found. This is then used to create a new plot with a `db_distance` that is closer to the estimated distance. This is iterated until the computed distance is close enough to `db_distance`. This scanning for the right distance is an operation that would only occur when the system has no previously known estimate of the LEDs and is scanning for them for the first time or when the LEDs are very close.

As an illustrative example, consider the LED to be 300 mm away. If the system starts by assuming the distance to be 1500 mm and generates the Δ plot to estimate

the angles, the estimated $\theta_{\mathrm{p},f.\mathrm{b}}$ and $\theta_{\mathrm{p},f.\mathrm{t}}$ will be further apart from each other than reality. Using these plots, the algorithm will try a distance that is even closer than 300 m. However, we can see that the error reduces with each iteration, making the problem convex.

To determine the absolute 3D position, the estimated values from the localization algorithm are used in:

$$\begin{aligned} \mathbf{v}_{f.\mathrm{b},x} &= \|\mathbf{v}_{f.\mathrm{b},x,y}\| \cdot \sin(\theta_{\mathrm{p},f.\mathrm{b}}) \cdot \cos(\theta_{\mathrm{y},f.\mathrm{b}}). \\ \mathbf{v}_{f.\mathrm{b},y} &= \|\mathbf{v}_{f.\mathrm{b},x,y}\| \cdot \sin(\theta_{\mathrm{p},f.\mathrm{b}}) \cdot \sin(\theta_{\mathrm{y},f.\mathrm{b}}). \\ \mathbf{v}_{f.\mathrm{b},z} &= \|\mathbf{v}_{f.\mathrm{b},x,y}\| \cdot \cos(\theta_{\mathrm{p},f.\mathrm{b}}). \end{aligned} \tag{3.11}$$

Here, $\|\mathbf{v}_{f.\mathrm{b},x,y}\|$ represent the horizontal estimated distance from the fishtail. Furthermore, the bottom LED is used as the reference point for the location of the fish, which is why $\theta_{\mathrm{p},f.\mathrm{b}}$ is used.

3.4 Classifying Confidence Levels

As seen in Fig. 3.6, the overlapping area between the diode pairs depends on the LED's horizontal distance from the receiver. Furthermore, both the top and bottom LEDs of a fishtail need to be in the overlapping area which essentially defines the FOV. Even within this area, the values towards the edges are inferred with more error as they have a low SNR with the weakest received power signal for one of the PDs. This is why we introduce a "Strength" label. In Fig. 3.7, the strength of all possible LED locations at a horizontal distance of 300 mm is displayed. This is calculated with Eq. (3.12), where $P_{\max\,\mathrm{S}}$ represents the highest power value that is expected to be measured for $10 \cdot \log(P_{\mathrm{r},i,j})$. The strength value can then indicate how confident a measurement is, with a numerical value between 0 and 1. This value would, for example, also be weaker when the scattering rate is very high, or the the LED is very far away. For a distance measurement, the minimum of the strength readings of the top and bottom LEDs is taken as the strength for that distance estimation. Since the distance will weaken the RSSR in an exponentially decaying relationship, the strength label will decrease linearly for the strongest signal received at a greater distance. This can be reduced to Eq. (3.13), where $P_{\max\,\mathrm{S}}$ can be adapted to make c equal to 1, and x is dependent on the medium.

$$\min_{i\in\{A,B,C\}} \left\{ \frac{10 \cdot \log(P_{\mathrm{r},i,j})}{10 \cdot \log(P_{\max\,\mathrm{S}})} \right\} \tag{3.12}$$

$$S = x \cdot d + c \tag{3.13}$$

Algorithm 1: Localization Algorithm

Data: $P_{\mathrm{r,meas},i,f.\mathrm{t}}$,$P_{\mathrm{r,meas},i,f.\mathrm{b}}$ $(\forall i \in \{A, B, C\})$
Result: $\|\mathbf{v}_{j,x,y}\|$, $\theta_{\mathrm{y},f.\mathrm{b}}$, $\theta_{\mathrm{p},f.\mathrm{b}}$

1 Initialize `db_distance` to 50cm;
2 Compute

$$10 \cdot \log\left(\frac{P_{\mathrm{r,meas},i,f.\mathrm{t}}}{P_{\mathrm{r,meas},k,f.\mathrm{t}}}\right),$$
$$10 \cdot \log\left(\frac{P_{\mathrm{r,meas},i,f.\mathrm{b}}}{P_{\mathrm{r,meas},k,f.\mathrm{b}}}\right)$$
$$\forall (i,k) \in \{(A,B),(A,C),(B,C)\}$$

;
3 **while** ***True*** **do**
4 Compute using `db_distance`

$$10 \cdot \log\left(\frac{G_{\mathrm{r}}(\theta_{i,j})}{G_{\mathrm{r}}(\theta_{k,j})}\right)$$
$$\forall (i,k) \in \{(A,B),(A,C),(B,C)\}$$

;
5 `total_diff` $= \sum_{(i,k)}$ |Line 2 - Line 4|;
6 `least_diff` = min(`total_diff` for f.t and f.b);
7 **if** *`least_diff`* $f.t$ *&* $f.b \leq$ *0.25* **then**
8 Extract $\theta_{\mathrm{y},f.\mathrm{b}}$, $\theta_{\mathrm{p},f.\mathrm{b}}$ from Line 4 using index of `least_diff`;
9 Calculate `distance` using Eq. (3.10);
10 **if** |*`distance`* - *`db_distance`*| $\leq$ *5 cm* **then**
11 STORE `distance`, $\theta_{\mathrm{y},f.\mathrm{b}}$, $\theta_{\mathrm{p},f.\mathrm{b}}$;
12 **END**;
13 **else**
14 `db_distance` += $\frac{1}{2}$ (`distance` - `db_distance`)
15 **else**
16 Outside of FOV, discard measurement;
17 **END**;

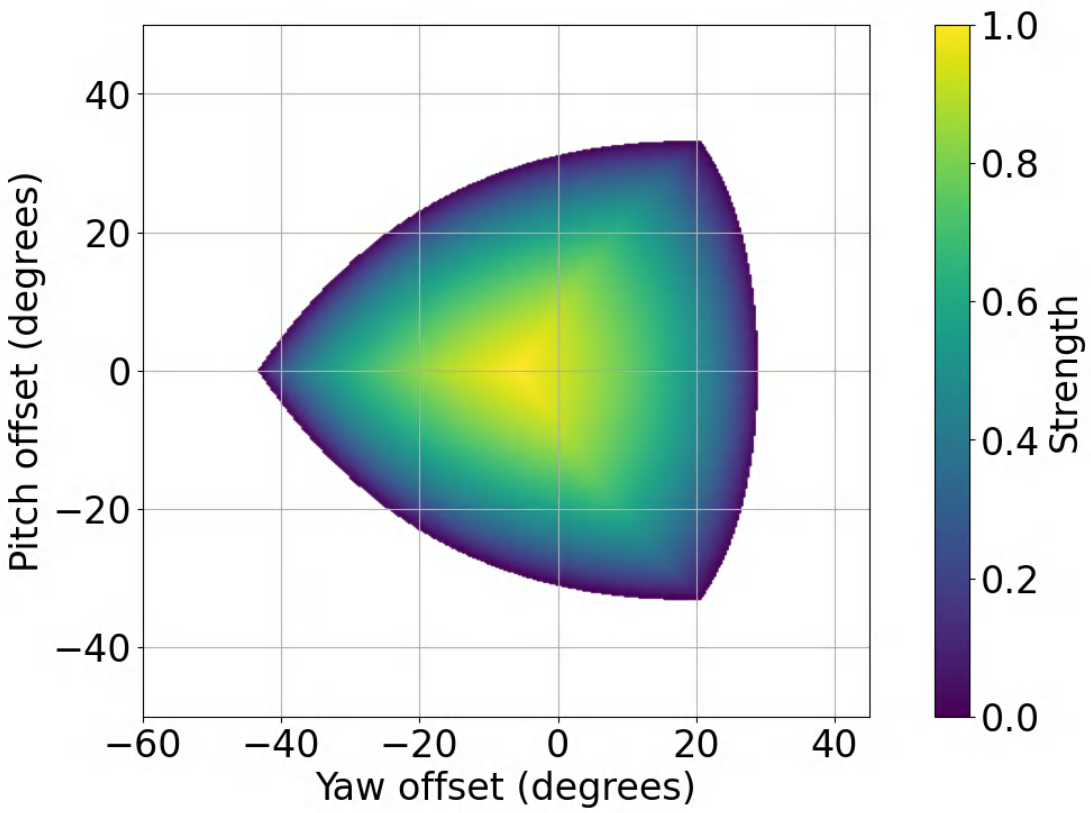

Figure 3.7: **Confidence value of the system for the bottom LED placed 300 mm away.**

Chapter 4

Intermediate Steps

In this chapter, the steps until the final localization system are described. First, a static LED with no modulation whatsoever was measured by the OPT101 module without ambient light, with varying the angle of the OPT101 and of the LED by the usage of steppers. The steppers with the LED and OPT101 attached can be seen in Fig. 4.1. To drive the steppers, the stepper driver chip a4988 was used. This would be connected to its separate 12V supply line and be controlled by the Teensy. The Teensy would additionally also sample the signals from the OPT101 photodiodes at the frequency of 40kHz.

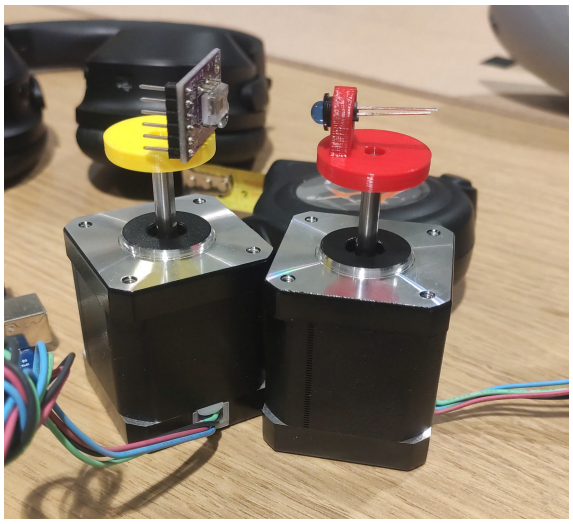

Figure 4.1: **Testing the response by varying angles at fixed distances.**

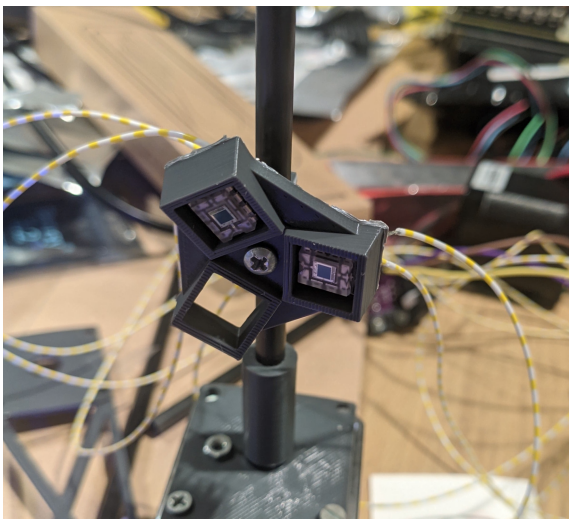

Figure 4.2: **Testing different PD receiver structures.**

Next, different structures were tested to see the response, while trying to put the OPT101 diodes closer together. A capture of this is shown in Fig. 4.2.

To test the 2D angles, custom GCODE was sent to a Prusa MK3S 3D printer. With the LED in attached to the printer head, and the receiver structure in a fixed position. This is shown in Fig. 4.3.

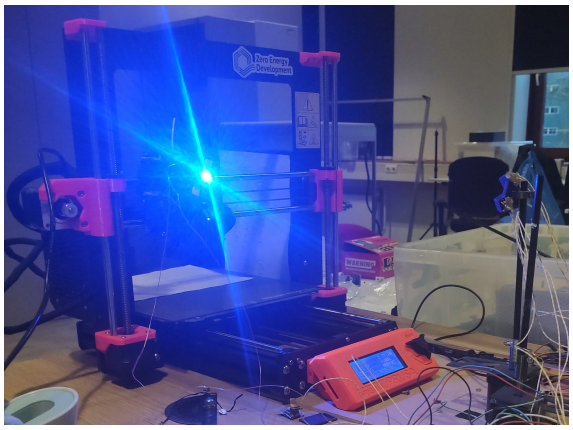

Figure 4.3: **The MK3S 3D printer with the LED in front of the receiver structure.**

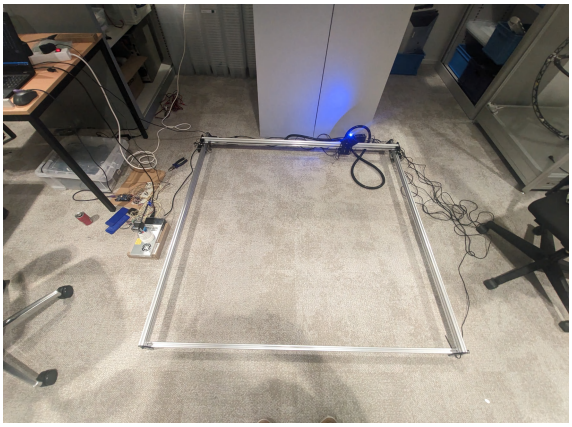

Figure 4.4: **The OpenBuilds system, assembled.**

To test both the 2D angles and distance, the OpenBuilds Acro 1515 was used. This is a 2D linear positioning system oftentimes used for tasks as engraving or milling. The build can be seen in Fig. 4.4. Here, the LED is attached to the head of the Acro 1515, and the receiver structure to the left of the build can turn around its own axis, simulating its yaw offset.

Then, to be able to tell apart different LED beacons, the application of different frequencies was applied on each LED. This result carried over well to the OPT101, and the Goertzel algorithm was implemented in the Teensy to get power components of those frequencies. The FFT of the signal is shown in Fig. 4.5.

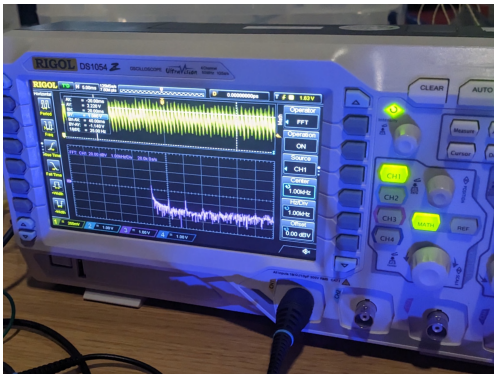

Figure 4.5: **Two LEDs on the oscilloscope, showing its FFT.**

The receiver structure was then poured in epoxy to waterproof the setup. Also, the LED has been made waterproof. Since the package of the OPT101 itself is already waterproof on the top, there was no need to cover the sensor part and alter the response. The epoxied photodiodes can be seen in Fig. 4.6 and the setup in the water in Fig. 4.7b.

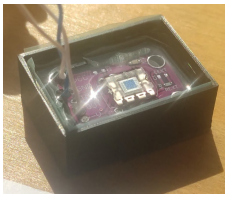

Figure 4.6: **The photodiode epoxied for its waterproofness.**

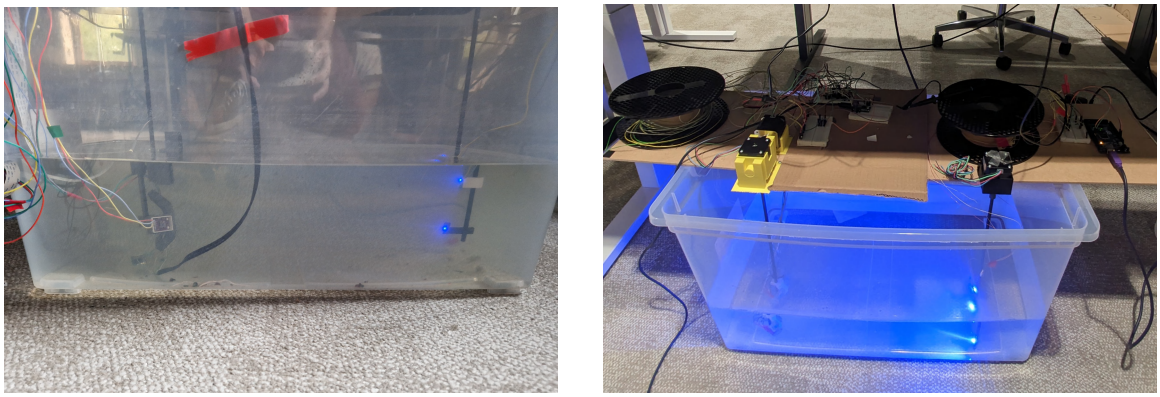

(a) **Side view** (b) **Angled view.**

Figure 4.7: **The waterproofed setup in a bucket of water.**

To create a more robust setup, a custom PCB was placed for both the LED driving circuit, as well as the stepper actuation and PD readout with the Teensy. The latter can be seen in Fig. 4.8.

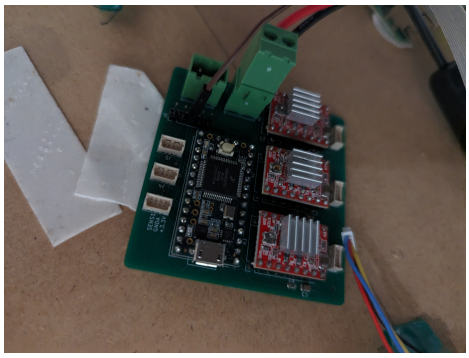

Figure 4.8: **The custom PCB with the Teensy, stepper drivers and connector interface.**

The Arducam OV5647 [1] was connected to a Raspberry Pi 4 for the possibility of testing the angles in an uncontrolled setup. Image tracking using OpenCV was then

applied to find the angles towards the LEDs. The output of this, with the reflections, can be seen in Fig. 4.9.

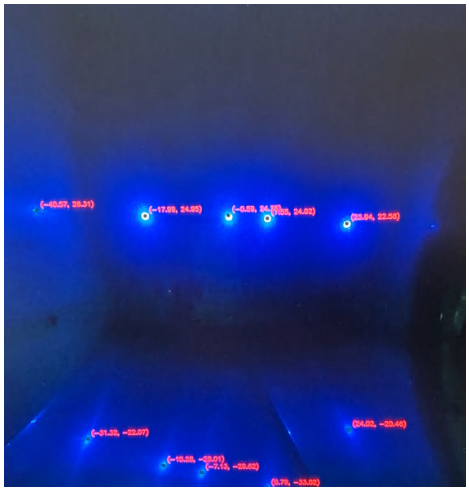

Figure 4.9: **The camera output, processed through OpenCV.**

The receiver structure was also updated to place in blue glass filters, to get more robustness to the ambient light and not saturate the PD. The updated structure can be seen in Fig. 4.10.

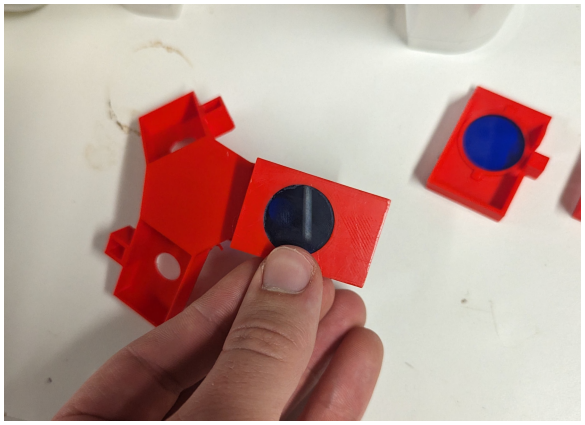

Figure 4.10: **Receiver structure with optical glass filters.**

As for the theoretical model, it was directly modelled but included all components of Eq. (3.4). This was done to test if the transmitter profile is indeed negligible with the distances that the setup would have.

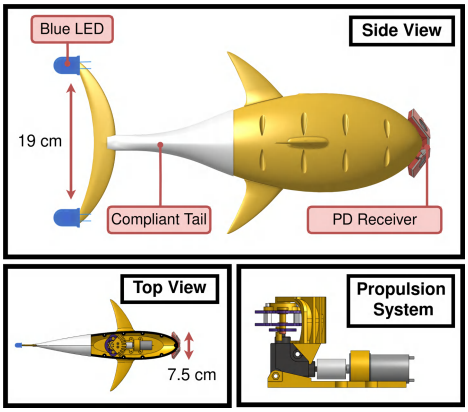

Figure 5.1: **Our localization system used in the OpenFish robots to augment them with joint localization and communication capabilities.**

Chapter 5

Localization System Design

5.1 Underwater Mobile Robotic Fishes

The localization system requires two blue 455 nm LEDs that constitute the transmitter to be placed on every underwater robot. If using a robotic fish-styled AUV, this would be placing one on each end of the tail. Additionally, a photodiode receiver structure is placed in front of the body of the AUV. This is depicted in Fig. 5.1. Every LED communicates with the receiver using a different ON-OFF frequency that the receiver uses to tell them apart. Using the method system described in Section 3.2.1, the receiver can tell which direction each LED is in. Combining the directions of two LED beacons that correspond to the same AUV with a known length of the tail (or vertical separation of the LEDs), the receiver can calculate the position of the target AUV in 3D.

The underwater mobile robot used in this work is based on the open-source soft

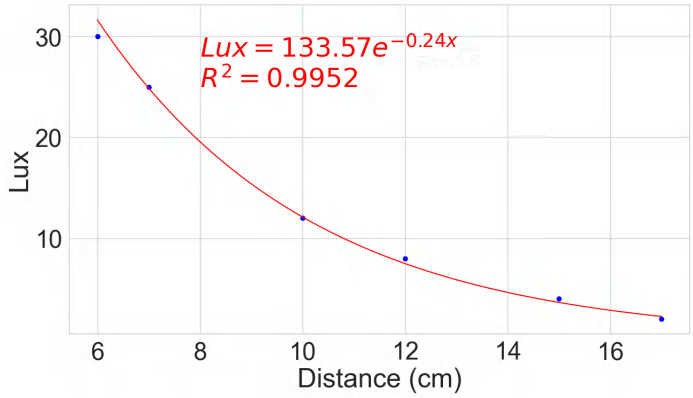

Figure 5.2: **Variation of Illuminance of one transmitter LED with distance.**

robotic fish - OpenFish design [12]. This bio-inspired robot is specially optimized for higher speed and efficiency. It features a DC motor that drives a soft tail segment accurately mimicking the thunniform swimming mode of real fish. Such robotic fishes are more advantageous than rotor-based AUVs as they do not create disturbing vibrations in the water, actively suck in objects or wildlife into the propeller and have higher power efficiency [8]. The higher speed and small size of these robots make them an ideal system that benefits from the features of our localization system.

5.2 Transmitter Design

Two mono-colour LEDs are used for the transmitters, with a half-intensity beam width of 125 degrees [22]. Its blue light has a wavelength of 455 nm, chosen for its high propagation through the water compared to other colours in clear water [42]. The transmitters are placed 19 cm vertically apart in the setup, the same distance as the length of the OpenFish tail. Placing the two LEDs apart makes it possible to triangulate the distance towards the tail if the direction towards both LEDs is known, as explained in Section 3.3. Due to the mechanics of the OpenFish, the tail is always expected to be vertical, never skewed in any direction. The LEDs on the tail will be oriented towards the back of the fish to keep the intensity highest towards the following fish behind it. A forward current of 5.5 mA is chosen, which clips the signal at the receiver PDs only at distances of 1 cm or closer when no ambient light is present. The Lux readings for the LED (in air) have been measured and are shown in Fig. 5.2. Note that the LED has been transmitting with a 50% ON-OFF Keying cycle. Different forward currents can, however, be chosen to create more Lumen at the transmitter. The forward current against Lumen plot can be found in Fig. 5.3.

Different frequencies up to 1.8 kHz can be applied to perform ON-OFF Keying of the LED using the microcontroller's PWM output. This limit is imposed as a

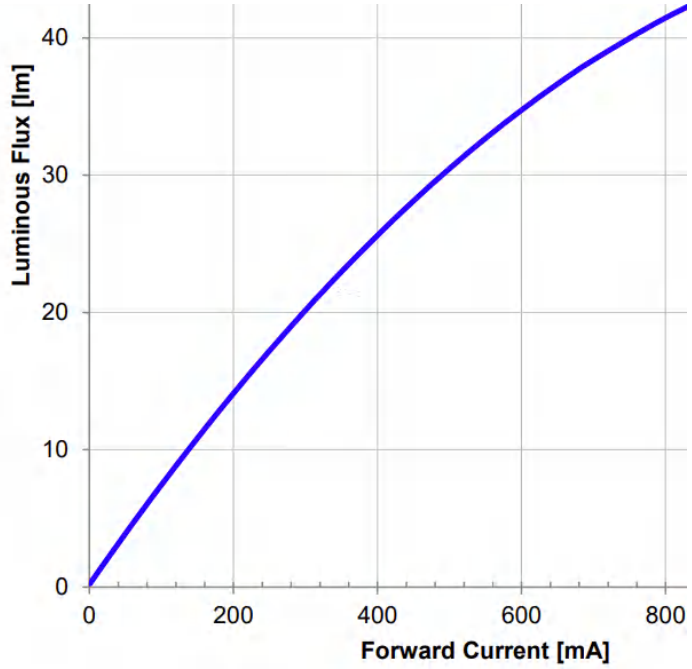

Figure 5.3: **Variation of luminous flux with forward current for a 455 nm ceramic waterclear LED [22].**

consequence of the photodiode circuit described in Section 5.3. A frequency gap of at least 50 Hz is needed between the flashing frequencies of the two LEDs to distinguish the signals at the receiver. This is also explained in Section 5.3. These different frequencies help distinguish each LED uniquely and thus are used to deduce the locations of the individual LEDs. Each fish robot uses LEDs to communicate its uniquely assigned beacon through the ON-OFF Keying method. The circuit diagram used to drive the LED can be found in Fig. 5.4.

5.3 Receiver Design

The receiver uses a tetrahedral-like 3-photodiode structure with each photodiode bent inside. This is depicted in Fig. 5.6. This structure uses the difference of angles of the PDs to deduce the individual locations of the LEDs, as explained in Chapter 3. Using Δ (RSSR) between each PD pair creates robustness to the medium that the light travels through [49]. The ideal ratio stays the same irrespective of the scatter and absorption rate of the medium, the only difference being in the noise level that is present when the signal is weaker. Varying the tilt between the DPs creates a trade-off between the FOV and the accuracy. A tilt of 35 degrees from the normal direction vector of the receiver was chosen for each PD. This results in the angle difference of

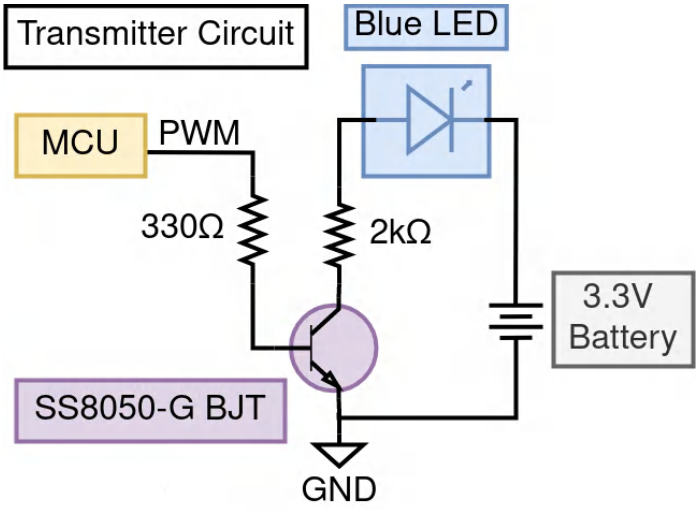

Figure 5.4: **Transmitter circuit showing how the blue LED is driven using a microcontroller PWM signal.**

60 degrees between each PD pair in Fig. 3.3. This choice gives us a FOV of around 60 degrees at 15 cm and 95 degrees horizontally at ¿1 m. The reasons for this design choice are explained in Section 3.2. An optical blue glass filter is placed in front of the diode to attenuate all other wavelengths of light and prevent full PD saturation when the fish is closer to the surface or another light source.

The OPT101, a monolithic photodiode with an on-chip trans-impedance amplifier, is used. It has a high responsivity, and the integrated combination of the photodiode and trans-impedance amplifier on a single chip eliminates issues like leakage current errors, noise pick-up, and gain peaking from stray capacitance. Its output voltage increases linearly with light intensity [30]. It is put in a configuration of 10x amplification by placing an external resistor for the feedback loop, the schematic for which can be found in Fig. 5.5. There is no possibility of fully saturating the PD with the LED in this configuration, but the bandwidth of the PD becomes 1.8 kHz. This is done to improve the SNR of the OPT101 since the responsivity increases linearly with the resistance and the noise with the square root of the resistance. The output from the three PDs is sampled at 40 kHz by a Teensy 3.2 micro-controller. The Goertzel FFT algorithm is applied to scan for the specific frequencies tied to each LED using bins of 400 samples. From this configuration, the bandwidth of the algorithm becomes $40000/400 = 100$ Hz [17]. The Goertzel algorithm has been chosen due to its lower computing complexity than full FFT algorithms since we are interested in only a portion of all frequencies. The resulting power components of these frequencies are then fed to the localization algorithm. The working of this functionality is explained in Section 3.3.

With the use of our algorithm, the relative 3D location of the other AUVs can be deduced as long as there is LOS between them. The further the LEDs are, the lower the SNR will be; this will translate to a more significant error and the need for averaging. With the current configuration of 1.8 kHz bandwidth at the PD, the system allows communication of additional data at this rate from each transmitter LED.

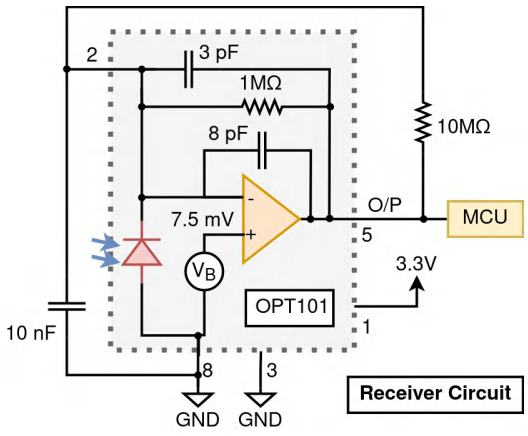

Figure 5.5: **Circuit schematic showing the OPT101 photodiode configuration used in the receiver.**

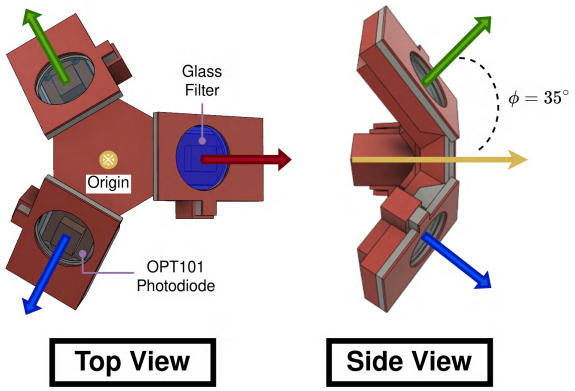

Figure 5.6: **Our receiver structure with a 35-degree difference between each PD's direction vector(green, blue, red arrows) and the normal vector of the structure (yellow arrow).**

Chapter 6

Evaluation and Results

6.1 Experimental Setup

A controlled test rig was created to test the performance of the localization system. The setup can be seen in Fig. 6.2. The fishtail and receiver are shown with half opacity to demonstrate the possible elevating and yawing motions. With this setup, all possible yaw and pitch offsets could be controlled. The stepper above the receiver can rotate the aluminium rod around its axis to create a specific yaw offset. The stepper above the fishtail can trolley up or down the fishtail, from which the desired pitch offset can be obtained. On the fishtail, two LEDs are connected, one at the top and one at the bottom, facing the receiver. The encasings of the steppers are mounted on a wooden plank and can be moved to the needed positions to measure at different distances. The wooden plank rests on the edges of a pool, and the rods are partly submerged in the water. The receiver was 25 cm below the water's surface. Both steppers are actuated by a Teensy 3.2, which is also connected to the three OPT101 PDs. The receiver structure can be seen in Fig. 6.1.

For collecting measurements, the Teensy can orient the receiver around its axis in a sweeping motion for different elevations of the transmitter. The PD signals are sampled at the Teensy and scanned for the power components corresponding to the beacon frequency of the top and bottom LED of the fishtail. These values are captured at different yaws, pitch offsets, and horizontal distances between the rod of the receiver and the fishtail. The blue LEDs on the transmitter communicate their ID using the beacon frequencies they have been assigned. This is controlled by an Arduino Atmega 2560 with an independent battery supply. For the results shown in Section 6.1.1, a sweep was done at the distances of 32, 34, 39, 59, 64, 87, and 99 cm. Due to the nature of the setup, limited elevation angles can be recorded at larger distances. This is also expected in the fish swarm scenario, where the vertical separation between fishes will not be extremely large.

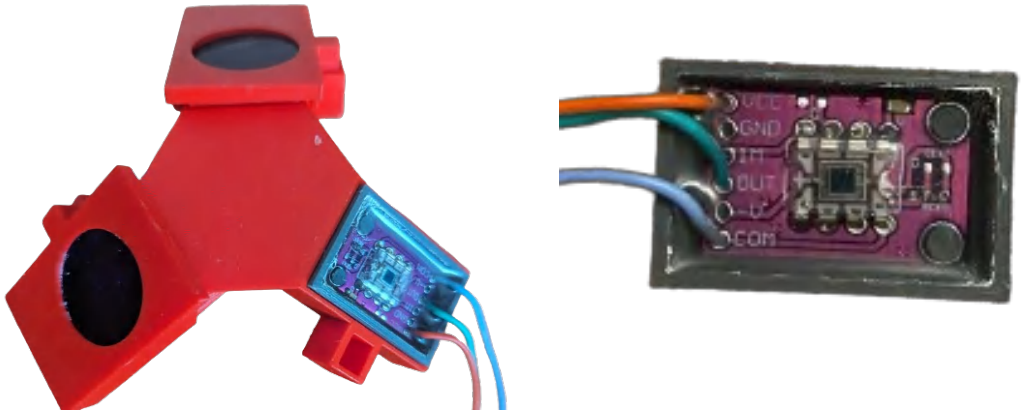

Figure 6.1: **Fabricated photodiode receiver structure with one glass filter removed (left) and the waterproofed OPT101 photodiode (right).**

For the validation of the localization algorithm and the calculation of the estimated fishtail location, underwater measurements were carried out in a 3 m diameter circular pool (Fig. 6.3). Most measurements were done without an overhead light. Measurements carried out in the presence of ambient light showed that it did not factor into the localization results. The setup in the water can be seen in Fig. 6.3, where the murkiness of the water is clearly visible.

6.1.1 Effect of Multipath and Noise

A sweep according to the procedure in Section 6.1 was done for different distances underwater. The received power for the distance of 32 cm for diode B is shown in Fig. 6.4. Here, a vertical smear can be seen that is caused by signal multipath. To test the algorithm's validity, the overhanging test rig is placed in different locations within the pool, which causes the system to experience different scenarios with the multipath effect. A plot similar to Fig. 3.6 is created for each distance; the results for 32 and 64 cm are shown in Fig. 6.5 and Fig. 6.6, respectively. Besides the effects of multipath highlighted in yellow in Fig. 6.5, the apparent effect of noise can be seen in Fig. 6.6. The dots at the edges of the 12 dB threshold highlight this.

6.1.2 Localization Performance

The positioning error was calculated to determine the performance. This is the Euclidian distance offset between the actual bottom of the fishtail and the estimated one by the localization algorithm. This positioning error is categorized using an absolute "Strength" confidence level (explained in Section 3.4) when all the received power values are evaluated using the localization algorithm. The result for one of the dis-

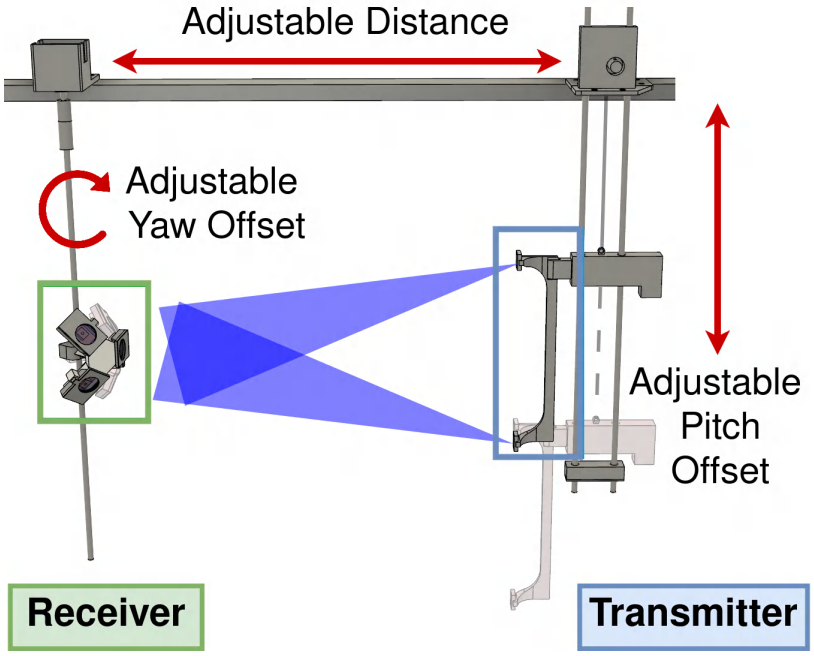

Figure 6.2: **Controlled experimental setup used to vary pitch, yaw and distance between the receiver (green) and the transmitter (blue).**

tances can be seen in Fig. 6.7. Note that the maximum error scale has been capped at 30 cm, with some errors reaching 2.5 meters. This is, however, in the region where the confidence level is low, as seen in Fig. 6.8. Combining this, all measured inputs can be used to estimate the position and used or discarded based on the confidence level. The confidence level correlates very well to what is in the FOV and what is not. But even within the strongest part of the confidence level, some error can be seen in Fig. 6.7. This is partly due to the multipath effect but can also be attributed to the inaccuracies of the diode layout structure and its gain profile. Combining the confidence level and the positioning error, CDF plots are made for three different distances (Fig. 6.9). Here, it can be seen that the strength level can be used to clearly distinguish performance, especially when the confidence drops below 0.55. The measurements were also averaged, but only for far distances (like 98 cm). This was beneficial as the received signals have a lower SNR at these distances. This can be seen in Fig. 6.10, where the measurements were taken ten times and averaged before using the localization algorithm. Using the confidence label, the measurements can estimate the position of the fishtail with an Mean Absolute Error (MAE) of 3.1 cm for the 32 cm distance and 39 cm for the 98 cm distance. This goes down to 29 cm for the ten times averaged measurement.

To gain more insight into the bias of the error, the measurements from the different

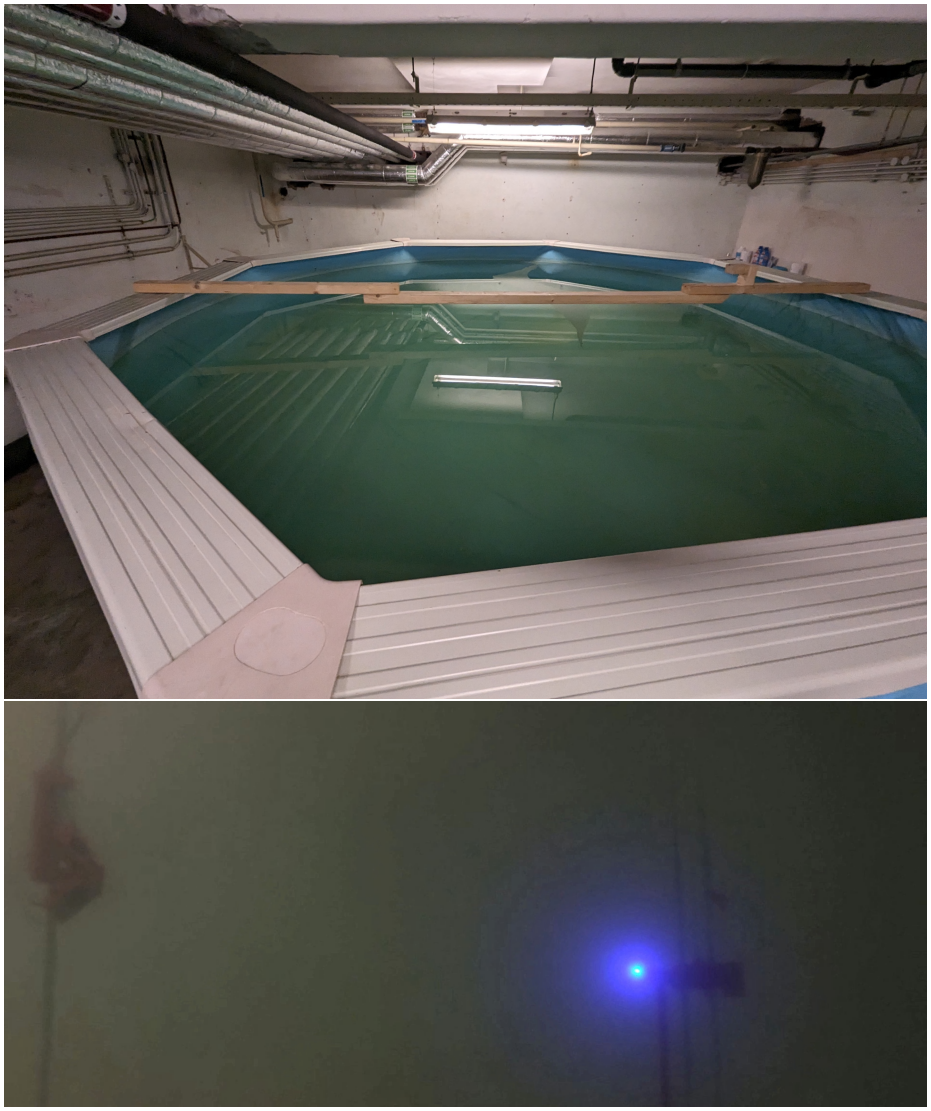

Figure 6.3: **Data collection and system evaluation were carried out in a 3 m wide indoor pool (top) using the submerged controlled test rig (below).**

distances were aggregated and converted to the relative error. In Fig. 6.11, this distribution of the relative distance error can be seen. Here, the distance error is divided by the actual measurement distance. The strength confidence levels below 0.5 and above 0.9 did not have enough samples to be included. It can be clearly seen that there is a bias, caused by the mismatch in the theory Δ plot and the measurement Δ plot.

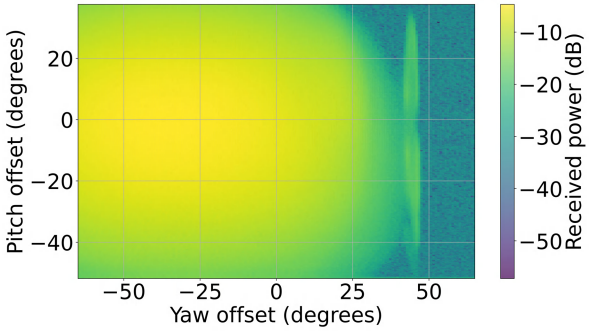

Figure 6.4: **Received power in dB at diode B when the bottom LED is at 32 cm distance.**

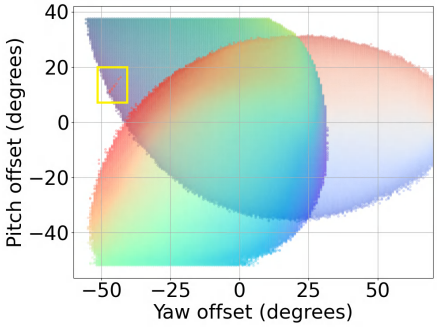

Figure 6.5: **Δ plot for each diode pair when the bottom LED is 32 cm away from the receiver.**

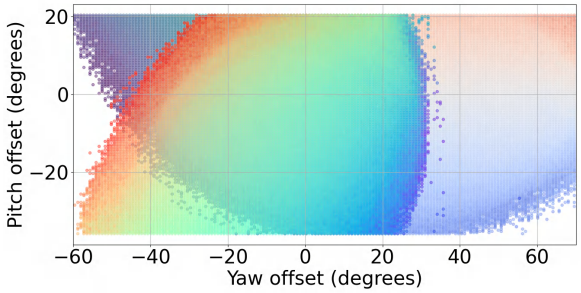

Figure 6.6: **Δ plot for each diode pair when the bottom LED is 64 cm away from the receiver.**

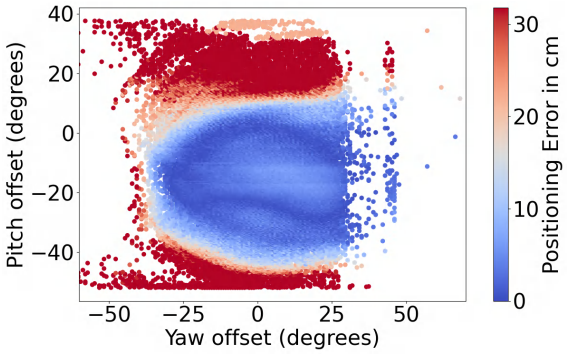

Figure 6.7: **Positioning error (in mm) from the localization algorithm at a transmitter-receiver distance of 32 cm.**

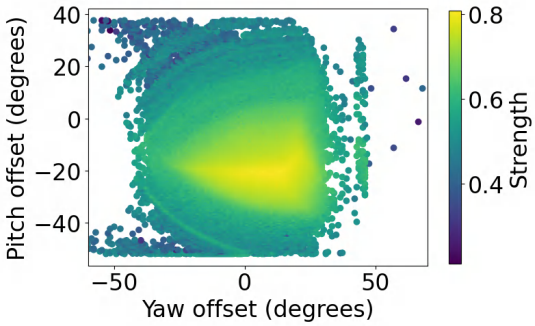

Figure 6.8: **Confidence levels of the estimated locations using our *Strength* metric when the transmitter and receiver are at a distance of 32 cm.**

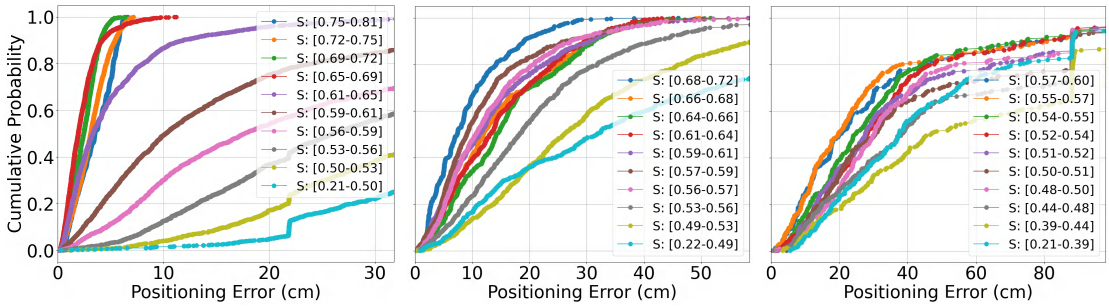

(a) **At 32 cm** (b) **At 58 cm** (c) **At 98 cm**

Figure 6.9: **Cumulative Distribution Function (CDF) plot of positioning error at different distances categorized by the strength confidence level (S).**

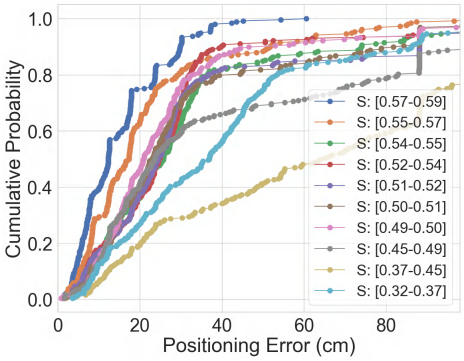

Figure 6.10: **CDF plot of the positioning error at 98 cm when the signal is averaged ten times categorized by the strength confidence level (S).**

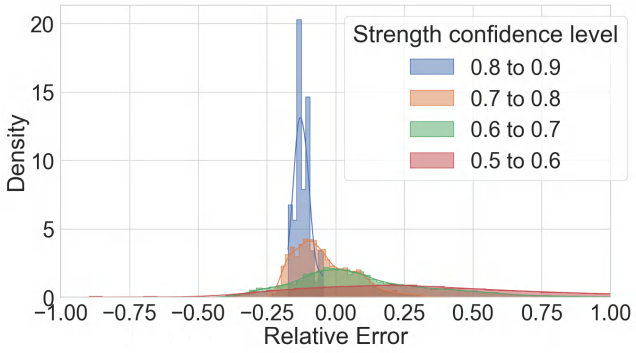

Figure 6.11: **Density distribution of Relative Error (RE).**

6.2 Strength

The Strength label would indicate when the LEDs from the fishtail are being received the strongest; thus, the receiver would be pointing as close as possible to the fishtail. This confidence level follows a logarithmic relationship to the received power, as seen in Eq. (3.12). This signal's exponential decay in water becomes linear for the strength confidence level. From all the distances measured, this resulted in the linear equation $S = -0.0039d + 1$, with S being the strength level and d is the distance in cm. This equation has been fitted to intersect $(0, 1)$ by adapting the $P_{\max S}$ value from Eq. (3.12). This fit had a coefficient of determination (R^2) of 0.9976.

Table 6.1: **Power consumption of system components**

System Components	**Power per Device (mW)**	**No. of Devices**	**Total Power (mW)**
LED circuit	18.8	2	37.6
OPT1010 photodiode	0.60	3	1.8
Arduino microcontroller	396	1	396
Teensy microcontroller	198	1	198

6.3 Power Consumption

The current consumption was measured for the transmitted (LED) and receiver (PD), the Arduino driving the transmitter, and the Teensy driving the receiver. The resulting power consumption is summarized in Table 6.1. The Arduino has been chosen for the test rig only; in the application, a single Teensy in an AUV would be connected to both the LEDs and the PDs. Note that the LED circuit and PD are only for one of each; the expected added power consumption would be 237 mW per AUV, which is still an order of magnitude lower than camera-based systems.

Chapter 7

Discussion

We presented our solution to underwater localisation for a swarm of small resource-constrained AUVs. Here, we discuss the applicability of the system and the points of possible improvement.

7.1 Environments

The OPT101 diode that the localisation system uses was measured outside water to characterise its fabrication parameters and incorporate them into the theoretical model. The estimated positioning accuracy of the system in dirty turbid water is found to be sufficiently high for it to be used in a feedback control loop with a Kalman filter to enable swarming behaviour. The system can be used in waters with different values of scattering and absorption rates by using only the signal strength. This can be done without any calibration and without a drop in accuracy. If the fish is used in even dirtier waters, the LED output intensity can tuned to be higher to increase the received strength received at the diodes. This will effectively increase the c constant in Eq. (3.13), creating a larger range where the receiver can follow the transmitting fish when pointed towards it. The blue glass optical filters ensure that the values at the diodes are not saturated in the presence of ambient light.

7.2 Applicability

This system can be applied to all robots that need inexpensive or high-speed short-range tracking within LOS for swarm behaviour. The absence of audio frequencies makes it possible to observe sea life without disturbing marine life affected by those frequencies. By using these high-frequency light signals, communication can also be combined in the same localisation channel. This way, the AUVs can also be used as high-speed communication links with a base station on shore. The most important

feature is that no calibration is needed for different mediums, with the system being immune to water turbidity and working in dirtier and clearer waters. If the expected medium is predominantly muddier waters, the blue LEDs can be swapped for green ones, which have less absorption for more shallow surfaces with dirty waters. Nothing would have to be changed then except for the optical filter and the transmitting LEDs.

7.3 Improving Communication

Currently, the system extracts the power components of different frequencies to know which LED beacon is received. This can directly work with On-Off-Keying (OOK), where the power component of that frequency would be affected in all PDs, keeping the RSSR the same. However, this means that every LED would need a different frequency with a frequency gap of 50Hz as explained in Section 5.3. A higher spectral efficiency can be achieved by using OFDM. A guard interval could be added to counter intersymbol interference (ISI) caused by the multipath effect. Also, the OPT101 can be made into a configuration with higher bandwidth at the cost of increased noise. This would enable the LED frequencies to be driven up to 58 kHz to achieve double the data rate (since every AUV will have two transmitting LEDs). However, then the system's sampling rate would also need to be adjusted appropriately to prevent aliasing.

7.4 Improving Localization

A 2D gain profile for each diode can be added to improve the localisation further. This will account for minor variations in the diodes that arise due to each diode's manufacturing process and can affect the diode's response to light rays hitting the die at varying angles. These rays have different scattering and refraction within the rectangular package. Power cycling or creating a standard higher LED intensity would also increase the SNR. In that case, the feedback loop gain should be adjusted, or a higher voltage range should be given to the OPT101 to prevent full saturation at close distances. A higher-quality optical glass filter can be used to reduce power loss at the blue wavelength. This filter could also be omitted if ambient light saturation is not to be expected. Although challenging, placing the PDs closer together could also be beneficial by reducing the small effect of the neglected components in Eq. (3.4). Also, information could be obtained even when the LED rays are only hitting one PD pair. Even though the position cannot be deduced, the area from which the LED rays originate can be calculated.

Another thing that could be done is to create an even higher tilt between the PDs at the cost of FOV, as explained in Section 3.2.1. The structure could be repeated over

the UAV as a more costly solution to regain the FOV. Although very challenging, the LED's power could be conserved by signalling to the other AUVs when localisation or communication is required. The AUV receiving these signals could then transmit its location towards the fish that requested it by having multiple LEDs but only activating the ones directed towards that specific AUV.

Chapter 8

Future Work and Conclusion

8.1 Future work

For future steps. A lot can be done with the past groundwork laid out. A full 360 degrees FOV can be made on the actual moving OpenFish with optionally higher accuracy by putting more receiver structures with a higher angle difference. A Kalman filter can be applied on the localization data and optionally be integrated with IMU data to extract speed and other data from the other UAVs. Besides this, the high bandwidth communication needs to be implemented in the same optical channel to evaluate its bit error rate (BER). Another improvement could be placing the diodes even closer by using a custom flexible PCB. This could eliminate even more the effects from the transmitter profile, and also reduce the amount of operations of finding the right distance. The latter would be the case because the plots at different distances of Fig. 3.6 would look more similar to one another.

8.2 Conclusion

We created a model for using AOA together with RSS, where the diodes do not necessarily need to be placed as close as possible to one another. This is done by the usage of finding the right distance iteratively by scanning the two vertical LEDs on each fishtail. We have established an optical localization link with multiple transmitters, with the possibility of extracting more information such as explicit but also implicit communication, due to the high speed of the optical link.

Bibliography

[1] Arducam 5MP OV5647 Ultra Wide Angle Fisheye Camera for Raspberry Pi.

[2] Nuno Abreu and Aníbal Matos. Minehunting Mission Planning for Autonomous Underwater Systems Using Evolutionary Algorithms. *Unmanned Systems*, 02(04):323–349, October 2014. Publisher: World Scientific Publishing Co.

[3] Saleha Al Al-Zhrani, Nada M Bedaiwi, Intesar F El El-Ramli, Abeer Z Barasheed, Ali Abduldaiem, Yas Al Al-Hadeethi, and Ahmad Umar. Underwater Optical Communications: A Brief Overview and Recent Developments. *Engineered Science*, 16:146–186, 2021.

[4] Ayshah S. Alatawi. A Testbed for Investigating the Effect of Salinity and Turbidity in the Red Sea on White-LED-Based Underwater Wireless Communication. *Applied Sciences*, 12(18):9266, January 2022. Number: 18 Publisher: Multidisciplinary Digital Publishing Institute.

[5] Alex Alcocer, Paulo Oliveira, and Antonio Pascoal. Study and implementation of an ekf gib-based underwater positioning system. *IFAC Proceedings Volumes*, 37(10):383–390, 2004.

[6] Alex Alcocer, Paulo Oliveira, and Antonio Pascoal. Underwater acoustic positioning systems based on buoys with gps. In *Proceedings of the Eighth European Conference on Underwater Acoustics*, volume 8, pages 1–8, 2006.

[7] Mohammad Furqan Ali, Dushantha Nalin K. Jayakody, and Yonghui Li. Recent Trends in Underwater Visible Light Communication (UVLC) Systems. *IEEE Access*, 10:22169–22225, 2022.

[8] Jamie M Anderson, K Streitlien, DS Barrett, and Michael S Triantafyllou. Oscillating foils of high propulsive efficiency. *Journal of Fluid mechanics*, 360:41–72, 1998.

[9] Prasad Anjangi, Amy Gibson, Manu Ignatius, Chinmay Pendharkar, Anne Kurian, Alan Low, and Mandar Chitre. Diver communication and localization system

using underwater acoustics. In *Global Oceans 2020: Singapore–US Gulf Coast*, pages 1–8. IEEE, 2020.

[10] Whitlow W. L. Au, Paul E. Nachtigall, and Jeffrey L. Pawloski. Acoustic effects of the ATOC signal (75 Hz, 195 dB) on dolphins and whales. *The Journal of the Acoustical Society of America*, 101(5):2973–2977, May 1997.

[11] Reza Barazideh, Wensheng Sun, Balasubramaniam Natarajan, Alexei V. Nikitin, and Zhaohui Wang. Impulsive Noise Mitigation in Underwater Acoustic Communication Systems: Experimental Studies. In *2019 IEEE 9th Annual Computing and Communication Workshop and Conference (CCWC)*, pages 0880–0885, Las Vegas, NV, USA, January 2019. IEEE Access.

[12] Sander C Van Den Berg, Rob B N Scharff, Z Rusák, and Jun Wu. OpenFish: Biomimetic design of a soft robotic fish for high speed locomotion. *HardwareX*, 2021.

[13] Florian Berlinger, Melvin Gauci, and Radhika Nagpal. Implicit coordination for 3D underwater collective behaviors in a fish-inspired robot swarm - MaM. *Science Robotics*, 6(50), 2021. Publisher: American Association for the Advancement of Science.

[14] Evandro Bernardes, Stéphane Viollet, and Thibaut Raharijaona. A Three-Photo-Detector Optical Sensor Accurately Localizes a Mobile Robot Indoors by Using Two Infrared Light-Emitting Diodes. *IEEE Access*, 8:87490–87503, 2020. Conference Name: IEEE Access.

[15] Josep Bosch, Nuno Gracias, Pere Ridao, Klemen Istenič, and David Ribas. Close-Range Tracking of Underwater Vehicles Using Light Beacons. *Sensors (Basel, Switzerland)*, 16(4):1–26, March 2016. Publisher: Multidisciplinary Digital Publishing Institute (MDPI).

[16] Thomas Casey, Brian Guimond, and James Hu. Underwater vehicle positioning based on time of arrival measurements from a single beacon. In *OCEANS 2007*, pages 1–8. IEEE, 2007.

[17] Michael Cerna and Audrey F Harvey. The Fundamentals of FFT-Based Signal Analysis and Measurement.

[18] Tuochao Chen, Justin Chan, Shyamnath Gollakota, and Paul G Allen. Underwater 3D positioning on smart devices. pages 33–48, September 2023. arXiv: 2307.11263 Publisher: Association for Computing Machinery (ACM) ISBN: 9798400702365.

[19] Xiuzhen Cheng, Haining Shu, Qilian Liang, and David Hung-Chang Du. Silent positioning in underwater acoustic sensor networks. *IEEE Transactions on vehicular technology*, 57(3):1756–1766, 2008.

[20] Mandar Chitre, Shiraz Shahabudeen, Lee Freitag, and Milica Stojanovic. Recent advances in underwater acoustic communications & networking. In *OCEANS 2008*, pages 1–10, September 2008. ISSN: 0197-7385.

[21] Peter Corke, Carrick Detweiler, Matthew Dunbabin, Michael Hamilton, Daniela Rus, and Iuliu Vasilescu. Experiments with Underwater Robot Localization and Tracking. In *Proceedings 2007 IEEE International Conference on Robotics and Automation*, pages 4556–4561, April 2007. ISSN: 1050-4729.

[22] Würth Elektronik eiSos GmbH. WL-SMDC SMT Mono-color Ceramic LED Waterclear 150353BS74500 Datasheet, December 2017. Publication Title: www.we-online.com.

[23] Christine Erbe. Effects of underwater noise on marine mammals. In *The effects of noise on aquatic life*, pages 17–22. Springer, 2012.

[24] Reza Ghaffarivardavagh, Sayed Saad Afzal, Osvy Rodriguez, and Fadel Adib. Underwater Backscatter Localization: Toward a Battery-Free Underwater GPS. In *Proceedings of the 19th ACM Workshop on Hot Topics in Networks*, pages 125–131, Virtual Event USA, November 2020. ACM.

[25] Josué González-García, Alfonso Gómez-Espinosa, Enrique Cuan-Urquizo, Luis Govinda García-Valdovinos, Tomás Salgado-Jiménez, and Jesús Arturo Escobedo Cabello. Autonomous Underwater Vehicles: Localization, Navigation, and Communication for Collaborative Missions. *Applied Sciences 2020, Vol. 10, Page 1256*, 10(4):1256, February 2020. Publisher: Multidisciplinary Digital Publishing Institute.

[26] Jason N. Greenberg and Xiaobo Tan. Dynamic Optical Localization of a Mobile Robot Using Kalman Filtering-Based Position Prediction. *IEEE/ASME Transactions on Mechatronics*, 25(5):2483–2492, October 2020. Publisher: Institute of Electrical and Electronics Engineers Inc.

[27] Jens M. Hovem. Ray Trace Modeling of Underwater Sound Propagation. In *Modeling and Measurement Methods for Acoustic Waves and for Acoustic Microdevices*. IntechOpen, August 2013.

[28] Huai Huang and Yahong Rosa Zheng. Aoa assisted localization for underwater ad-hoc sensor networks. In *OCEANS 2016 MTS/IEEE Monterey*, pages 1–6. IEEE, 2016.

[29] Dinh Quang Huy, Nicholas Sadjoli, Abu Bakr Azam, Basman Elhadidi, Yiyu Cai, and Gerald Seet. Object perception in underwater environments: a survey on sensors and sensing methodologies. *Ocean Engineering*, 267:113202, January 2023.

[30] Texas Instruments Incorporated. OPT101 Monolithic Photodiode and Single-Supply Transimpedance Amplifier, June 2015.

[31] Benjamin Kuch, Giorgio Buttazzo, Elaine Azzopardi, Martin Sayer, and Arne Sieber. Gps diving computer for underwater tracking and mapping. *Underwater Technology*, 30(4):189–194, 2012.

[32] Philip Lacovara. High-Bandwidth Underwater Communications. *Marine Technology Society Journal*, 42(1):93–102, March 2008.

[33] Hanjiang Luo, Yiyang Zhao, Zhongwen Guo, Siyuan Liu, Pengpeng Chen, and Lionel M Ni. Udb: Using directional beacons for localization in underwater sensor networks. In *2008 14th IEEE International Conference on Parallel and Distributed Systems*, pages 551–558. IEEE, 2008.

[34] Miquel Massot-Campos and Gabriel Oliver-Codina. Optical Sensors and Methods for Underwater 3D Reconstruction. *Sensors*, 15(12):31525–31557, December 2015. Number: 12 Publisher: Multidisciplinary Digital Publishing Institute.

[35] Farshad Miramirkhani and Murat Uysal. Visible Light Communication Channel Modeling for Underwater Environments With Blocking and Shadowing. *IEEE Access*, 6:1082–1090, 2018. Conference Name: IEEE Access.

[36] Jim Partan, Jim Kurose, and Brian Levine. A Survey of Practical Issues in Underwater Networks. *ACM SIGMOBILE Mobile Computing and Communications Review*, 11:17–24, November 2006.

[37] Qin Qin, Yi Tian, and Xin Wang. Three-dimensional uwsn positioning algorithm based on modified rssi values. *Mobile Information Systems*, 2021:1–8, 2021.

[38] Umair Mujtaba Qureshi, Zuneera Aziz, Faisal Karim Shaikh, Zuneera Aziz, Syed M.Zafi S. Shah, Syed M.Zafi S. Shah, Adil A. Sheikh, Emad Felemban, and Saad Bin Qaisar. RF Path and Absorption Loss Estimation for Underwater Wireless Sensor Networks in Different Water Environments. *Sensors 2016, Vol. 16, Page 890*, 16(6):890, June 2016. Publisher: Multidisciplinary Digital Publishing Institute.

[39] Scott Reed, Jon Wood, and Chris Haworth. The detection and disposal of IED devices within harbor regions using AUVs, smart ROVs and data processing/-fusion technology. In *2010 International WaterSide Security Conference*, pages 1–7, Carrara, Italy, November 2010. International WaterSide Security Conference. ISSN: 2166-1804.

[40] W John Richardson, Charles R Greene Jr, Charles I Malme, and Denis H Thomson. *Marine mammals and noise*. Academic press, 2013.

[41] Paul Rigby, Oscar Pizarro, and Stefan Williams. Towards geo-referenced AUV navigation through fusion of USBL and DVL measurements. pages 1–6, October 2006.

[42] Giuseppe Schirripa Spagnolo, Lorenzo Cozzella, and Fabio Leccese. Underwater Optical Wireless Communications: Overview. *Sensors 2020, Vol. 20, Page 2261*, 20(8):2261, April 2020. Publisher: Multidisciplinary Digital Publishing Institute.

[43] M. Stojanovic. Recent advances in high-speed underwater acoustic communications. *IEEE Journal of Oceanic Engineering*, 21(2):125–136, April 1996. Conference Name: IEEE Journal of Oceanic Engineering.

[44] Robert H. Tyler, Thomas B. Sanford, and Martyn J. Unsworth. Propagation of electromagnetic fields in the coastal ocean with applications to underwater navigation and communication. *Radio Science*, 33(4):967–987, 1998. _eprint: https://agupubs.onlinelibrary.wiley.com/doi/pdf/10.1029/98RS00748.

[45] Lixuan Wang and Caili Guo. Indoor visible light localization algorithm with multi-directional PD array. *2017 IEEE Globecom Workshops, GC Wkshps 2017 - Proceedings*, 2018-January:1–6, January 2018. Publisher: Institute of Electrical and Electronics Engineers Inc. ISBN: 9781538639207.

[46] Yongjin Wang, Bingcheng Zhu, Julian Cheng, and Zhiming Zhu. Optimal Optical Omnidirectional Angle-of-Arrival Estimator With Complementary Photodiodes. *Journal of Lightwave Technology, Vol. 37, Issue 13, pp. 2932-2945*, 37(13):2932–2945, July 2019. Publisher: IEEE.

[47] L.L. Whitcomb. Underwater robotics: out of the research laboratory and into the field. In *Proceedings 2000 ICRA. Millennium Conference. IEEE International Conference on Robotics and Automation. Symposia Proceedings (Cat. No.00CH37065)*, volume 1, pages 709–716, San Francisco, CA, USA, 2000. IEEE.

[48] Yinghao Wu, Xuxiang Ta, Ruichao Xiao, Yaoguang Wei, Dong An, and Daoliang Li. Survey of underwater robot positioning navigation. *Applied Ocean Research*, 90:101845, September 2019.

[49] Se Hoon Yang, Hyun Seung Kim, Yong Hwan Son, and Sang Kook Han. Three-dimensional visible light indoor localization using AOA and RSS with multiple optical receivers. *Journal of Lightwave Technology*, 32(14):2480–2485, July 2014. Publisher: Institute of Electrical and Electronics Engineers Inc.

[50] Xiaohui Yu, Jianping Wang, and Huimin Lu. Single LED-Based Indoor Positioning System Using Multiple Photodetectors. *IEEE Photonics Journal*, 10(6), December 2018. Publisher: Institute of Electrical and Electronics Engineers Inc.

[51] Zhaoquan Zeng, Shu Fu, Huihui Zhang, Yuhan Dong, and Julian Cheng. A Survey of Underwater Optical Wireless Communications. *IEEE Communications Surveys & Tutorials*, 19(1):204–238, 2017.

[52] Shijie Zhu, Xinwei Chen, Xiaoyan Liu, Guoqi Zhang, and Pengfei Tian. Recent progress in and perspectives of underwater wireless optical communication. *Progress in Quantum Electronics*, 73:100274, September 2020.